

1 **An assessment of GPS velocity uncertainty in California**
2

3 **Christopher W. Johnson^{1*}, Nicholas Lau¹, and Adrian Borsa¹**

4 ¹Scripps Institution of Oceanography, University of California San Diego, La Jolla, California,
5 92093, USA

6 * Now at Los Alamos National Laboratory

7 Corresponding author: Christopher W. Johnson (cwj004@ucsd.edu)
8
9

10 **Key Points:**

- 11 • Systematic review of California GPS positions and the published and derived velocities
12 using data from 5 different analysis centers.
- 13 • Published uncertainties show variability between analysis centers, are underreported, and
14 do not reflect the true velocity uncertainties.
- 15 • Vertical rates for individual stations differ up to 5 mm/yr, with systematic differences in
16 areas of highest subsidence and uplift.
17

18 Abstract

19 We analyze 580 continuous GPS stations in California from 5 analysis centers to quantify the
20 uncertainty in published velocities and develop a composite velocity for each station. The
21 horizontal positions are similar but the reported velocity varies by time series algorithm. Vertical
22 rates for individual stations differ up to 5 mm/yr, with systematic differences in some areas. The
23 published uncertainties show variability between analysis centers and are underreported,
24 suggesting these formal errors do not reflect the true velocity uncertainties. Differences by a
25 factor of 4 are found in the vertical and is comparable to deformation rates. An interpolated
26 ensemble vertical velocity field is developed and regions with the highest rates of uplift or
27 subsidence correspond to the largest variance in velocities between analysis centers, but high
28 station density can reduce these uncertainties. Applications that rely on sub-centimeter GPS
29 accuracy should consider the inherent uncertainty in published vertical velocity rate estimates.

30

31 Plain Language Summary

32 The continuous recordings from geodetic grade GPS sensors provides high resolution ground
33 motion measurements. Multiple analysis centers process the raw GPS data into daily station
34 positions and provide high quality data to the scientific community. Each analysis center applies
35 different processing techniques and model corrections that produces differences in the final time
36 series product. We analyze the GPS positions and published velocities for 5 analysis centers and
37 develop a composite velocity dataset with uncertainties for 580 stations in California. The
38 published positions are reevaluated to calculate a standardized velocity using 2 methods to assess
39 if the differences arise from the underlying positions or the time series analysis. We find the
40 horizontal positions are consistent but the vertical positions, which are an order of magnitude
41 less, vary by analysis center and the greatest discrepancies are in areas of the largest observed
42 subsidence. We further evaluate the vertical velocity field from all 5 analysis centers and develop
43 an ensemble velocity field to characterize the spatially varying uncertainty. Our results
44 demonstrate the importance of assessing position uncertainty using multiple analysis centers
45 when informing geophysical models of observed ground motions.

46 1 Introduction

47 Global positioning system (GPS) instruments and processing techniques provide
48 measurements with sufficient precision to quantify sub-centimeter geologic deformation (e.g.
49 Dixon, 1991). The technological capabilities of GPS spurred efforts to design a permanent GPS
50 network for continuous monitoring of the tectonic plate boundary in the western U.S. (Silver et
51 al., 1998), ultimately realized by the construction of the Plate Boundary Observatory (PBO)
52 between 2002 and 2012. The PBO network contains about 1,100 continuously recording GPS
53 stations at a median spacing of ~20 km and contributes most of the regional geodetic
54 observations used by the scientific community. Daily station positions and long-term velocities
55 for these stations are freely and openly available (Blewitt et al., 2018; Herring et al., 2016),
56 eliminating the need for user processing of raw GPS data and greatly expanding data access
57 across multiple disciplines (EarthScope O&M Proposal; GAGE Facility Proposal). Increasing
58 the diversity of GPS data users justifies the existence of the PBO network and demonstrates the
59 value of the GPS infrastructure for scientific, government, and commercial activities (Leveson,
60 2009).

61 More than a decade of daily GPS observations from the PBO network have provided
62 high-precision time series that constrain both short and long-term crustal motion in the western
63 U.S. This dataset is dominated by a broad zone of deformation extending from the Pacific Coast
64 to the western edge of the Rocky Mountains showing large horizontal displacements (median 21
65 mm/y). Strain localization on multiple faults across the region (e.g. Zeng et al., 2018) delineates
66 crustal blocks whose tectonic motion is estimated at 10-45 mm/yr (e.g. Simpson et al., 2012).
67 The dense station spacing and continuous recording enable quantification of spatiotemporally
68 heterogeneous motion associated with volcanic activity, uplift and subsidence, and postseismic
69 deformation (Hammond et al., 2016), whose vertical velocities are an order of magnitude smaller
70 (median <1 mm/yr) than the horizontal. The largest contribution to vertical displacements in
71 many areas is the solid earth elastic response to the hydrological cycle, which exhibits
72 seasonality and non-stationarity from changes in terrestrial water storage (Argus et al., 2017;
73 Borsa et al., 2014; Fu et al., 2015; Johnson et al., 2017).

74 Daily station positions and long-term velocities for most western U.S. stations are
75 estimated by multiple analysis centers using different processing algorithms, reference frames,
76 troposphere and tidal corrections, and time-series analysis techniques (Herring et al., 2016). Each
77 analysis center provides uncertainty estimates for their data products, but formal uncertainties
78 calculated for geodetic datasets can underestimate time-correlated error in position data and
79 usually do not characterize variance introduced by different processing assumptions (Herring et
80 al., 2016). Here, we leverage the published data products from 4 different analysis centers and
81 analyze the empirical uncertainties across the dataset. We focus on GPS station velocities, since
82 these are widely used and available. Our goals are to 1) quantify the observed uncertainty in 5
83 sets of published station velocities, 2) quantify differences between observed and published
84 uncertainties, 3) assess the extent velocity differences are consistent with different velocity
85 estimations versus consistent with different underlying GPS positions, and 4) assess whether the
86 variability in published velocity solutions is random or correlated with the degree of active
87 surface deformation.

88 **2 Published GPS products**

89 We analyze three-component North/East/Up (NEU) daily GPS positions and the
90 associated secular velocity estimates from 4 analysis centers: the Geodesy Advancing
91 Geosciences and EarthScope (GAGE) at Massachusetts Institute of Technology, Scripps Orbit
92 and Permanent Array (SOPAC) at Scripps Institution of Oceanography, NASA Jet Propulsion
93 Laboratory (JPL) in Pasadena, CA, and Nevada Geodetic Laboratory at the University of Nevada
94 Reno (UNR). These 4 centers produce 5 independent position/velocity datasets (or “solutions”),
95 which are the basis of the analysis. We occasionally refer to the north and east together as the
96 “horizontal” directions and the up as the “vertical” direction.

97 The “GAGE” solutions in our analysis (Herring et al., 2016) were produced using
98 GLOBK software to combine independent daily position solutions generated by the GAMIT
99 (Herring et al., 2015) and GIPSY OASIS II (Zumberge et al., 1997) packages. SOPAC and JPL
100 provide independent position solutions to the NASA MEASURES Solid Earth Science Data
101 Records project. The “MEASURES-JPL” solution is processed using GIPSY and the
102 “MEASURES-SOPAC” solution is processed using GAMIT, and a combination of both
103 solutions (Bock et al., 1997) is available from NASA as the “JPL” solution. The “UNR” solution
104 is produced by the Nevada Geodetic Laboratory, which uses GIPSY to process daily positions

105 for >17,000 GPS stations around the globe (Blewitt et al., 2018). While only 2 software packages
106 are used, each analysis center parameterizes its processing in a unique way and applies different
107 auxiliary models and assumptions (e.g. to characterize atmospheric delay along the signal path
108 from GPS satellite to GPS station). Furthermore, each analysis center applies a different
109 algorithm to estimate published station velocities.

110 Our study considers 580 GPS stations located in a tectonically active region of the
111 western U.S.A. (30.25° to 41.25°N, 118.25° to 121.0°E). We use published position time series
112 and velocities in the IGS08 reference frame for these stations for all 5 solutions (GAGE,
113 MEASURES-SOPAC, MEASURES-JPL, JPL, and UNR; see Supporting Information). The start
114 time, and therefor the timespan, of the position data is variable for each solution, with many PBO
115 sites coming online in 2006, and the end time is early 2019 when the records were accessed.
116 Additionally, we produce two standardized velocity datasets by uniformly applying two of the
117 velocity estimation techniques (described below) to daily positions from each of the analysis
118 centers using the entire record of published solutions. This allows us to separately attribute the
119 variability in published velocities to differences between 1) position estimates and 2) velocity
120 algorithms.

121 **3 GPS preprocessing and time series analysis**

122 3.1 Removal of offsets and outliers in GPS position time series

123 Decadal-length continuous GPS time series such as those we analyze in this study
124 typically include one or more step-like offsets caused by equipment changes or earthquakes,
125 position outliers from system or environmental noise, and/or temporal gaps from equipment
126 malfunction or scheduled maintenance. We use metadata provided by the Nevada Geodetic
127 Laboratory (Blewitt et al., 2018) to provide the time of potential offsets for each GPS station,
128 assuming that any remaining offsets are insignificant. We model potential offsets as a Heavyside
129 step function in all three coordinate directions, which we scale by the difference between the
130 median positions of the 14 days before and after the offset time. We subtract all estimated offsets
131 for each GPS station to generate offset-corrected time series for further analysis.

132 To identify outliers in each station time series, we calculate and remove a 6-month
133 moving average from offset-corrected NEU positions, then calculate the median-average-
134 deviation of the residuals in each coordinate direction. Outliers are defined as epochs whose
135 residual value in any coordinate direction exceeds 5 times the associated deviation. The 6-month
136 window length is selected to capture expected seasonal and longer-period signals, while
137 identifying shorter-period variability (e.g. periodic snow cover on GPS antennas) in the outlier
138 estimation. Outliers, which typically occur at a few isolated days, are replaced by their
139 corresponding values from the 6-month moving average. Since our analysis of velocities does
140 not require complete time series, we do not estimate or otherwise provide position values for
141 time series gaps.

142 3.2 Time-series velocity estimates

143 We use two methods to generate NEU velocity estimates for the 5 published position
144 solutions. The first method (“MIDAS”) applies the non-parametric MIDAS algorithm, which
145 utilizes median statistics to estimate robust velocities from the offset/outlier-corrected time series
146 (Blewitt et al., 2016). The second method (“parametric”) obtains velocities from Equation 1.

$$x(t) = c_1 + c_2 t + \sum_{n=1}^2 (a_n \sin 2\pi n t + b_n \cos 2\pi n t) \quad (1)$$

The observed time series $x(t)$ is modeled as a mean value c_1 , a linear velocity $c_2 t$, and annual and semiannual sinusoids with coefficients (a_1, b_1) and (a_2, b_2) , respectively. While we do not use the sinusoid terms in our analysis, including them in the model ensures that our velocity estimates are not biased for time series that span a non-integer number of sinusoidal cycles. We solve Equation 1 using robust linear least squares to derive model coefficients that minimize the misfit between the observed and modeled time series.

3.3 Ensemble GPS vertical velocity field

We use the GPS imaging method (Hammond et al., 2016) to estimate the vertical velocity field associated with station velocities from each analysis center, interpolating the results onto a uniform 0.1° grid (Figure S1a-e). Working with velocity fields rather than individual stations mitigates the impact of station-specific noise, which can obscure the underlying spatial structure of deformation (Hammond et al., 2016; Kreemer et al., 2018). We create an ensemble velocity field for California (Figure S1f) whose individual realizations are estimated by randomly selecting a velocity value for each GPS station from one of the 5 analysis centers. The process is repeated 1000 times and the mean of all iterations for each grid cell is the ensemble velocity field and the standard deviation estimates the uncertainty. The results do not considerably change when using more iterations.

4 Results

4.1 Solutions for each processing center

4.1.1 Published velocities

To assess aggregate differences between analysis centers, we compare the published GPS station velocities for each station relative to the mean of the station velocities from all five centers (henceforth “mean velocity”). Our analysis uses the robust sample statistics of the station-by-station residuals calculated by subtracting the mean velocity from published velocities in the NEU directions. We use the median of the residuals to evaluate their central tendency and assign the robust standard deviation (SD) of the residuals to 0.74 of the interquartile range, to quantify the dispersion (Table 1). Residual velocities relative to their mean range from -0.12 to 0.17 mm/yr in the north and -0.10 to 0.06 mm/yr in the east. Similarly, SDs range from 0.19 to 0.26 mm/yr in the north and 0.15 to 0.21 mm/yr in the east. Vertical velocities are more variable than the horizontal, with median values ranging from -0.26 to 0.30 mm/yr and the SD ranging from 0.33 to 0.74 mm/yr.

The distributions of the north and east velocity residuals (Figure S2a/b) show thin tails with 95% of the residuals between ± 1 mm/yr, corresponding to the lower SDs reported and indicating good agreement between the analysis centers published horizontal velocities. There is more variability in the up distributions (Figure S2c), with 88% of the residuals ranging between ± 1 mm/yr. The GAGE vertical velocities are positively shifted and JPL is negatively shifted relative to the mean, while the others are a factor of 3 smaller. The JPL vertical residuals have the broadest distribution (0.74 mm/yr SD) and no clear central peak.

Table 1. Summary statistics for published, parametric, and MIDAS velocities from 5 analysis centers. The statistics are reported as the median of the velocity residuals (relative to the analysis centers mean) \pm the residual robust standard deviation (1σ) in units of mm/yr.

	Published Velocities (mm/yr)			Parametric Velocities (mm/yr)			MIDAS Velocities (mm/yr)		
	North	East	Up	North	East	Up	North	East	Up
GAGE	0.17 \pm 0.22	-0.10 \pm 0.20	0.30 \pm 0.49	0.14 \pm 0.10	-0.05 \pm 0.09	0.47 \pm 0.29	0.11 \pm 0.09	-0.01 \pm 0.10	0.36 \pm 0.22
SOPAC	-0.01 \pm 0.26	0.05 \pm 0.17	-0.08 \pm 0.35	-0.08 \pm 0.07	0.01 \pm 0.09	-0.07 \pm 0.25	-0.12 \pm 0.09	0.04 \pm 0.09	0.09 \pm 0.19
MEAS-JPL	-0.12 \pm 0.19	-0.04 \pm 0.15	-0.08 \pm 0.33	-0.01 \pm 0.08	-0.02 \pm 0.07	-0.01 \pm 0.24	-0.01 \pm 0.08	-0.04 \pm 0.08	-0.02 \pm 0.18
JPL	-0.02 \pm 0.24	0.06 \pm 0.21	-0.26 \pm 0.74	-0.06 \pm 0.11	0.06 \pm 0.09	-0.34 \pm 0.25	0.02 \pm 0.08	0.01 \pm 0.07	-0.34 \pm 0.22
UNR	-0.02 \pm 0.20	0.02 \pm 0.17	0.08 \pm 0.44	-0.00 \pm 0.09	-0.01 \pm 0.09	-0.05 \pm 0.28	-0.00 \pm 0.07	-0.01 \pm 0.07	-0.07 \pm 0.23

186

187 The cumulative distribution functions (CDFs) of the published velocities (Figure 1a/c/e)
188 are visually consistent and the distributions are equivalent according to Kolmogorov-Smirnov
189 tests for all pairs of analysis center NEU solutions. Unlike the CDFs of the velocities themselves,
190 the CDFs of reported uncertainties (Figure 1b/d/f) show considerable variability between
191 analysis centers, with much greater differences in the vertical than in the horizontal (by a factor
192 of ~ 4). In the horizontal, reported uncertainties for the top 30% (east) to 50% (north) of all
193 stations are systematically less than our own empirical uncertainty estimate, defined as the
194 standard deviation (1σ) of the 5 solutions and shown as the black dashed line in the rightmost
195 panels in Figure 1. In the vertical, reported uncertainties are more consistent with empirical
196 uncertainties. The UNR and JPL solutions provide the largest and most realistic uncertainty, with
197 only 25% of the reported uncertainty less than the empirical assessment. We note the UNR
198 reported uncertainty is scaled by a factor of 3 from the calculated value so it is similar to root-
199 mean-square accuracy (Blewitt et al., 2016). The CDFs of velocity uncertainties show that
200 GAGE, MEASURES-SOPAC, and MEASURES-JPL consistently report lower uncertainties
201 than the other analysis centers. Overall, we find that published horizontal uncertainties are
202 underreported relative to our empirical uncertainty estimate, and vertical uncertainties vary by
203 analysis center.

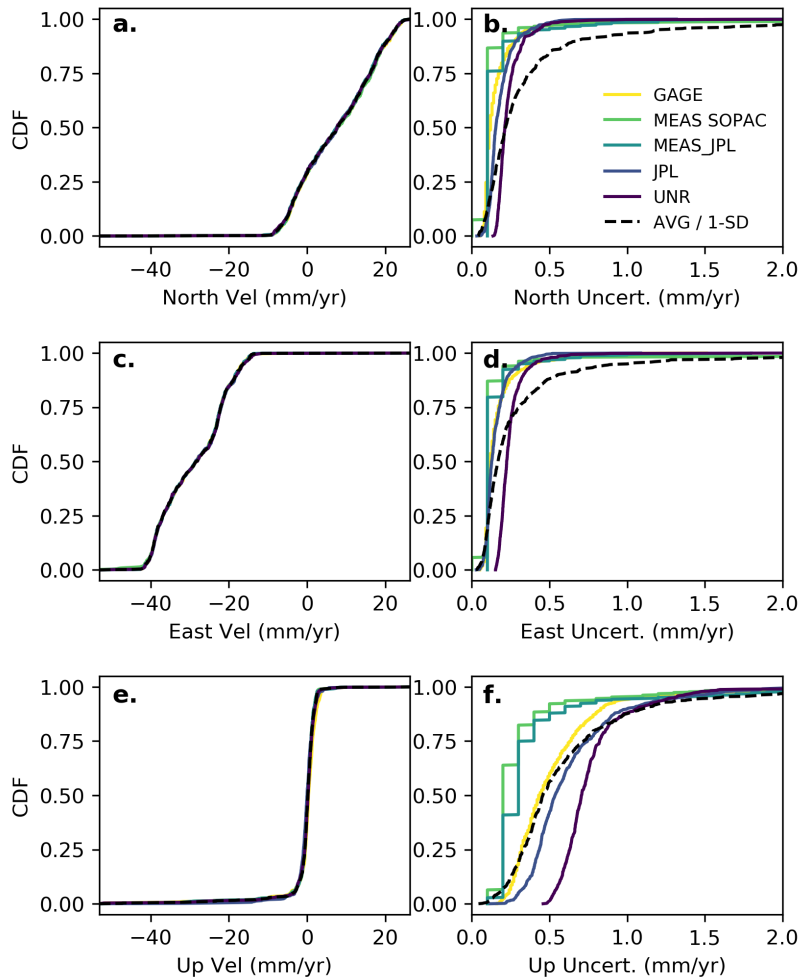


Figure 1. Cumulative distribution functions (CDFs) for the published velocities of the 5 processing centers and reported uncertainties for north (**a** and **b**), east (**c** and **d**), and up (**e** and **f**). The black dashed line indicates the CDF of the mean station velocities (in panels **a**, **c**, and **e**) and the CDF of the 1σ uncertainties of the station velocities (in panels **b**, **d**, and **f**).

204 4.1.2 Station velocity reanalysis

205 To understand factors contributing to the velocity differences between analysis centers,
 206 we reprocess the GPS station velocities for each center using the two methods described in
 207 Section 3.2. Reprocessing velocities using MIDAS reduces the variance (1σ) by $\sim 50\%$ and
 208 narrows the range of the residual distributions to about half the values for the published
 209 velocities (Figure S3, Table 1). Re-estimating velocities using the time series model in Equation
 210 1 also reduces variance of the residuals relative to the published velocities, but not to the same
 211 extent as the MIDAS algorithm (Figure S4, Table 1). The offsets in the means of the up residuals
 212 are present in all three velocity estimates (Figures S2c, S3c, S4c) and are a result of the vertical
 213 scale estimates applied by each analysis center when obtaining the daily positions (see Herring et
 214 al., 2016).

215 4.2 Vertical velocity assessment

216 4.2.1 Comparison of station velocities in regions of active deformation

217 Individual station velocities, averaged across all five analysis centers, reveal clear
 218 patterns of deformation across California that serve as context for our analysis below (Figure 2;
 219 Dataset S1). The northern Coast Ranges show subsidence of ~ 1 mm/yr while the central Coast
 220 Ranges and Sierra Nevada show uplift of ~ 2 mm/yr. The Central Valley is subsiding at >50
 221 mm/yr from commercial agriculture groundwater pumping (Faunt et al., 2016) and shows the
 222 largest uncertainties in vertical velocity rates. In southern California, south of the Transverse
 223 Range, the velocities show a mix of uplift and subsidence that is attributed to tectonic loading
 224 and anthropogenic aquifer usage (Argus et al., 2005; Howell et al., 2016). The overall pattern of
 225 uplift and subsidence across California is consistent with previous studies of GPS vertical rates
 226 (Amos et al., 2014; Hammond et al., 2016), but we identify stations with high velocity
 227 uncertainty as reflected in the scatter of published velocity values. Those high-uncertainty GPS
 228 stations are primarily located in the high-rate subsidence regions of the Central Valley, Los
 229 Angeles basin, and Salton Trough.

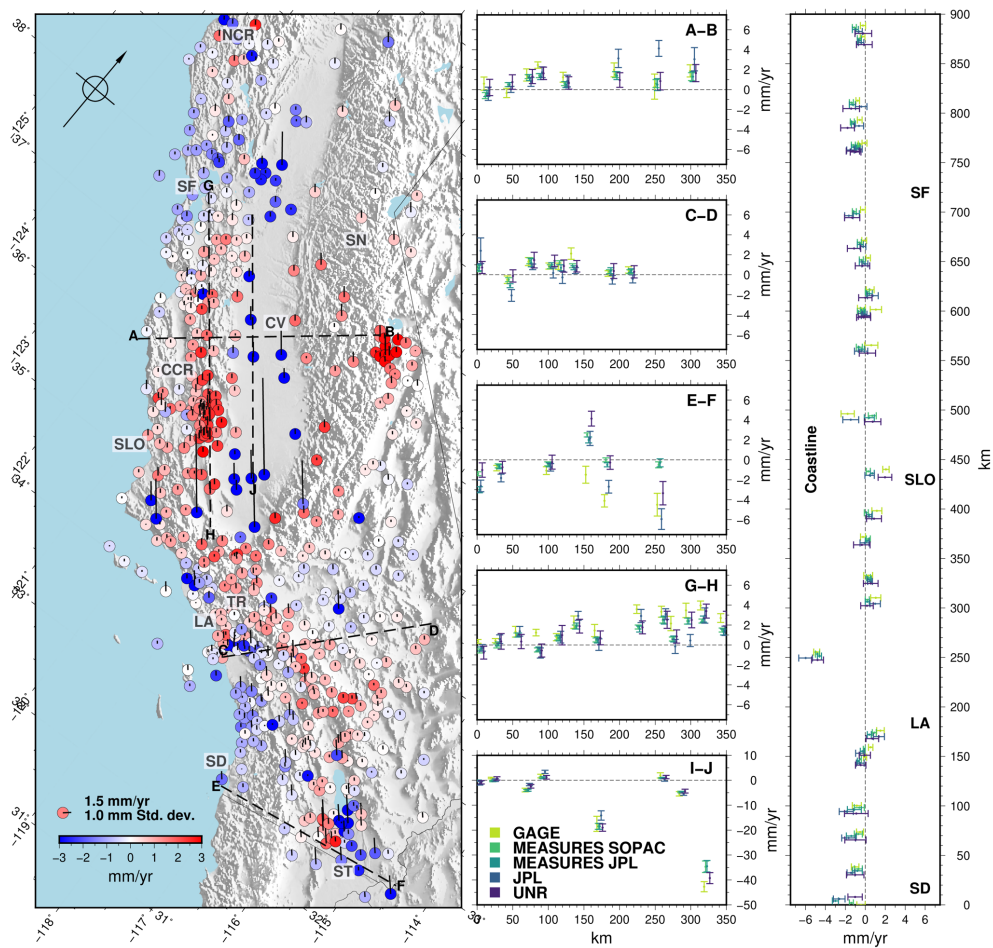


Figure 2. GPS vertical velocities for 5 published processing centers along the coastline and five linear transects in actively deforming regions of California. In the left panel, circle colors indicate published station velocities and the tick mark lengths indicate 1σ uncertainties. In the middle panels, circles and error bars indicate published velocities and 1σ uncertainties. The dashed black lines in the left panel correspond to the ~ 350 km transects shown in the middle panels. The right panel shows GPS station velocities along the California coast with specific labeled for reference (SF-San Francisco, SLO-San Luis Obispo, LA-Los Angeles, SD-San Diego, CV-Central Valley, TR-Transverse Range, SN-Sierra Nevada, NCR-North Coast Range, CCR-Central Coast Range, ST-Salton Trough).

230 Vertical velocities along five 350 km transects highlight the differences in the published
 231 velocities for areas of known deformation from tectonic, hydrological, and anthropogenic
 232 sources (Figure 2). Transect A-B extends from the central Coast Ranges to the Sierra Nevada,
 233 excluding measurements in the Central Valley with rapid subsidence. It shows slight subsidence
 234 at the coastline, uplift in the Coast Ranges (0.5 to 3.0 mm/yr), and general uplift in the Sierra
 235 Nevada (-1.0 to 5.0 mm/yr). Of note, JPL's published velocities for the three stations on the
 236 eastern half of the transect are anomalously high by 1~4 mm/yr and uniformly exceed the 1σ
 237 uncertainty of the velocity estimates for all other analysis centers.

238 Transect C-D extends across the Los Angeles basin, crosses the San Andreas fault, and
 239 extends into the Mojave Desert. Subsidence in the Los Angeles basin (down to -2.0 mm/yr) is
 240 most pronounced near the San Gabriel Mountains, and there is almost no vertical motion in the
 241 Mojave Desert. On this transect, JPL published velocities diverge from those of other analysis
 242 centers by 1~2 mm/yr, lying outside the 1σ uncertainty of the other velocities for six of eight
 243 stations.

244 Transect E-F extends along the southern U.S. border from San Diego to Yuma, CA,
 245 traversing a region of active extensional tectonics. The coastal region shows subsidence (-3.5 to
 246 0.0 mm/yr), the Salton Trough near Brawley, CA shows uplift (1.0 to 5.0 mm/yr), and the eastern
 247 Salton Trough shows subsidence (-7.0 to 0.0 mm/yr). This transect is the most problematic from
 248 the standpoint of consistency between analysis centers. Four of the 6 GPS station exhibit velocity
 249 scatter involving two or more analysis centers and the range of velocities for individual stations
 250 (up to 6 mm/yr) is unusually high.

251 Transect G-H extends north-south along the central Coast Ranges from San Francisco to
 252 the southern San Joaquin Valley, following the Hayward-Calaveras-San Andreas Fault system. It
 253 shows ~ 1.0 mm/yr subsidence in the north, with increasing uplift moving south (-1.0 to 4.5
 254 mm/yr). There is some scatter of published velocities, but the uplift trend is similarly represented
 255 by all five analysis centers. GAGE velocities are consistently higher than other analysis center
 256 velocities along the transect, with the greatest differences (~ 1 mm/y) toward the south.

257 Transect I-J extends north-south through the Central Valley with rates to the north near
 258 0.0 mm/yr and strong subsidence (-45.0 to -10.0 mm/yr) at stations in the southern Central
 259 Valley caused by agricultural groundwater pumping. While the 2 stations on the transect
 260 exhibiting rapid subsidence have the largest scatter in absolute velocity of any station in our
 261 analysis, the difference relative to the 1σ velocity uncertainty is better than many other stations.

262 Motivated by the importance of correctly quantifying vertical land motion near coastal
 263 communities in the context of ongoing sea-level rise (National Research Council, 2012), we also
 264 examine a transect along the Pacific Coast of California south of Cape Mendocino. The 27
 265 stations in Figure 2 (right panel) show subsidence between San Diego and southern Los Angeles

266 (-3.0 to 0.0 mm/yr), transitioning to uplift in northern Los Angeles (0.0 to 2.0 mm/yr). Between
267 Los Angeles and San Luis Obispo, subsidence (-6.0 mm/yr) is observed near the agricultural
268 region of Oxnard (250 km), transitioning to a moderate uplift (-1.0 to 3.0 mm/yr). North of San
269 Luis Obispo there is little vertical motion until the San Francisco area, where we observe
270 subsidence (-2.0 to 0.0 mm/yr).

271 Vertical land motion along California's coast are rarely zero and exhibits areas of local
272 subsidence that can exceed sea level rise by a factor of 2, exacerbating the impact of rising ocean
273 waters. The variability in vertical estimates can be the same order of magnitude as sea level rise,
274 most clearly at stations near San Diego (0~100 km) and San Luis Obispo (450~500 km). This
275 suggests that information about vertical land motion, which is required to inform mitigation
276 efforts to combat rising waters, is dependent on sources whose inconsistencies can result in very
277 different conclusions about what actions may be needed.

278 4.2.1 Velocity field uncertainty

279 We use the ensemble velocity field (Figure 3a) and its associated uncertainties (Figure
280 3b) to highlight regions where differences in analysis center velocities could have the greatest
281 impact on the geophysical interpretation of vertical velocity rates. The dominant features are
282 observed in each analysis center velocity field, but vary spatially with amplitudes differences >3
283 mm/yr (Figure S1). The highest uncertainties in California are associated with the large-scale
284 subsidence of the southern Central Valley from groundwater pumping for agriculture (Faunt et
285 al., 2016). Subsidence is observed by all analysis centers (Figure S1), however the large
286 variability in reported velocities (Figure 2, transect I-F) and relatively low station density (Figure
287 3c) both contribute to elevated uncertainties. Another area of high uncertainty is the Salton
288 Trough, which is also subsiding. Median station distance in this area is low (<10 km), indicating
289 that the uncertainty originates entirely from the high variability in station velocity (Figure 2,
290 transect E-F).

291 The highest uplift rates in California are located in the Sierra Nevada (Figure 3a), a
292 region of somewhat elevated uncertainty (>0.50 mm/yr) that is characterized by low station
293 density and increased uncertainty that results from the anomalously high JPL estimates (Figure 2,
294 transect A-B). However, relatively high uplift rates to the west of the Central Valley are not
295 associated with increased uncertainty. Overall, regions with the highest rates of uplift or
296 subsidence correspond to the largest variance in velocities between analysis centers, but high
297 station density (e.g. to the west of the southern Central Valley) can reduce these uncertainties.

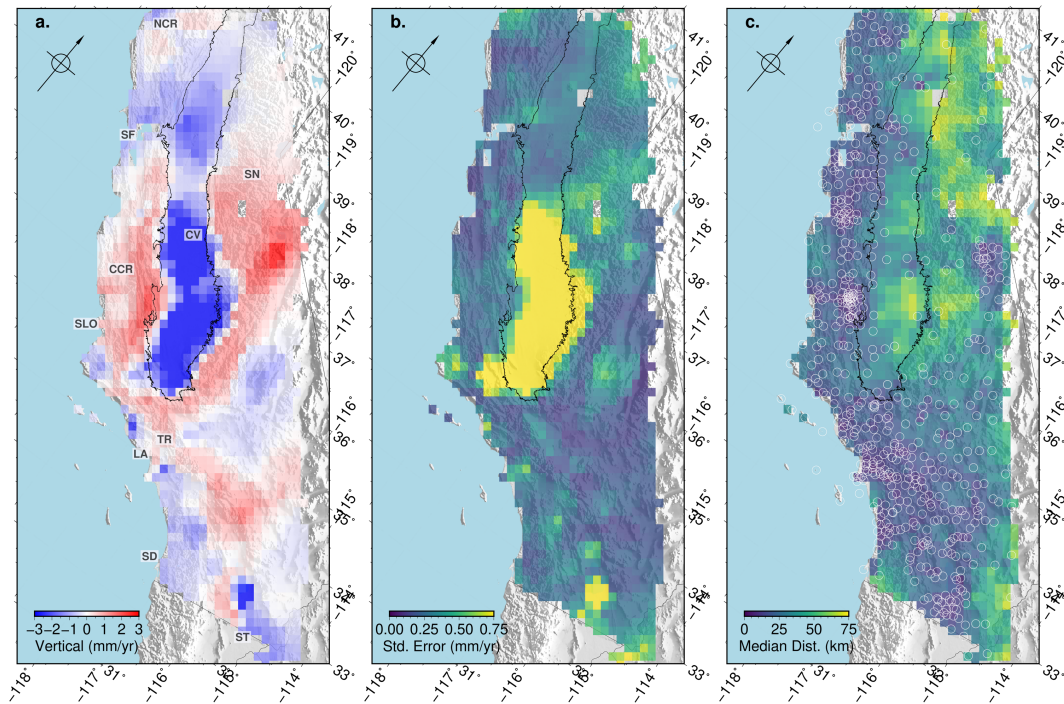


Figure 3. (a) The ensemble vertical velocity field and (b) standard error computed from all processing center solutions. (c) The median distance to GPS stations (white circles) used in imaging each grid; any grid cell with median distance >75 km is removed. The contour outline encompasses the Central Valley where stations are subsiding at rates much greater than -3 mm/yr. Location labels as in Figure 2.

298 5 Discussion and Conclusions

299 We analyzed NEU velocities for 580 GPS stations in California, comparing velocity
 300 estimates and their corresponding uncertainties from five GPS analysis centers. Taken as a
 301 whole, the velocity datasets from different analysis centers are statistically compatible. However,
 302 we find differences in vertical rates for individual stations of up to 5 mm/yr between analysis
 303 centers, and we document systematic differences in velocities along some transects. Our analysis
 304 in Section 4.1.2 shows that these differences arise about equally from different velocity
 305 estimation algorithms and different position time series. Velocity differences have implications
 306 for the physical interpretation of observed crustal deformation (Figure 2), and care should be
 307 taken when using velocities from a single analysis center. One concern is for geophysical models
 308 that use uncertainties to weight observations without accounting for the variability introduced by
 309 analysis center. An ensemble velocity field such as the one we introduce in Section 3.3
 310 represents one way to reconcile discrepancies in velocity estimates.

311 The inconsistent reported uncertainties between analysis centers are much larger than the
 312 velocities differences themselves. Some are expected based on differences in the methodologies
 313 (e.g. Blewitt et al., 2016; Herring et al., 2016) or the applied scale height estimates for the
 314 vertical positions (Herring et al., 2016). However, systematic differences are observed in areas of
 315 the highest subsidence and uplift (Figure 3), suggesting there are underlying incompatibilities in
 316 velocity estimation for these regions. A complication with estimating vertical velocities is the
 317 interannual variability in station positions observed as time series increase in length. This non-

318 linear ground motion can result from changes in terrestrial water storage (e.g. Borsa et al., 2014),
319 varying intensity of groundwater usage and recharge (e.g. Neely et al., 2020), and tectonic
320 signals (e.g. Hammond et al., 2018). Both the Central Valley (groundwater) and the Salton
321 Trough (tectonics, groundwater), which we highlight as regions of high variability in vertical
322 velocities, are impacted by strong non-linear surface deformation.

323 This study provides an independent estimate of NEU velocity uncertainty from the spread
324 between analysis center solutions, both for individual stations and for the ensemble velocity
325 field. We find that published station horizontal velocity uncertainties are systematically smaller
326 than our estimates, while published vertical uncertainties are analysis center dependent.
327 Furthermore, the ensemble uncertainty (Figure 3b) shows that there is a clear spatial pattern in
328 empirical velocity uncertainty. These observations strongly suggest that formal errors from
329 analysis centers do not reflect the true uncertainties of velocity estimates. Ensemble uncertainty
330 estimates, such as the one we introduce here, may provide more realistic values. We conclude
331 that science applications that rely on sub-centimeter GPS accuracy (e.g. assessing sea level rise,
332 InSAR correction and alignment, or hydrogeodetic water storage estimates) should carefully
333 consider and mitigate the inherent uncertainty in published vertical velocity rate estimates.

334 **Acknowledgments and Data**

335 We thank Debi Kilb for insightful comments that improved the manuscript. This material is
336 based upon work supported by the National Science Foundation EAR Postdoctoral Fellowship
337 award 1725344 which supported CWJ. The GPS data products were last accessed 1 April 2019:
338 GAGE from <ftp://data-out.unavco.org/pub/products/>; MEASURES SOPAC and MASURES JPL
339 from <ftp://garner.ucsd.edu/pub/timeseries/measures/ats/>; UNR from
340 <http://geodesy.unr.edu/index.php>; JPL from
341 https://sideshow.jpl.nasa.gov/pub/JPL_GPS_Timeseries/repro2018a/post/point. The composite
342 data sets are available as Supplementary Material Dataset S1.
343

344 **References**

- 345 Amos, C. B., Audet, P., Hammond, W. C., Burgmann, R., Johanson, I. A., & Blewitt, G. (2014).
 346 Uplift and seismicity driven by groundwater depletion in central California. *Nature*,
 347 *509*(7501), 483-486. doi:10.1038/nature13275
- 348 Argus, D. F., Heflin, M. B., Peltzer, G., Crampé, F., & Webb, F. H. (2005). Interseismic strain
 349 accumulation and anthropogenic motion in metropolitan Los Angeles. *Journal of*
 350 *Geophysical Research: Solid Earth*, *110*(B4). doi:10.1029/2003jb002934
- 351 Argus, D. F., Landerer, F. W., Wiese, D. N., Martens, H. R., Fu, Y., Famiglietti, J. S., et al.
 352 (2017). Sustained Water Loss in California's Mountain Ranges During Severe Drought
 353 From 2012 to 2015 Inferred From GPS. *Journal of Geophysical Research: Solid Earth*,
 354 *122*(12), 10,559-510,585. doi:10.1002/2017jb014424
- 355 Blewitt, G., Hammond, W. C., & Kreemer, C. (2018). Harnessing the GPS data explosion for
 356 interdisciplinary science. *Eos Trans. AGU*, *99*. doi:10.1029/2018EO104623
- 357 Blewitt, G., Kreemer, C., Hammond, W. C., & Gazeaux, J. (2016). MIDAS robust trend
 358 estimator for accurate GPS station velocities without step detection. *Journal of*
 359 *Geophysical Research: Solid Earth*, *121*(3), 2054-2068. doi:10.1002/2015jb012552
- 360 Bock, Y., Wdowinski, S., Fang, P., Zhang, J., Williams, S., Johnson, H., et al. (1997). Southern
 361 California Permanent GPS Geodetic Array: Continuous measurements of regional crustal
 362 deformation between the 1992 Landers and 1994 Northridge earthquakes. *Journal of*
 363 *Geophysical Research: Solid Earth*, *102*(B8), 18013-18033. doi:10.1029/97jb01379
- 364 Borsa, A. A., Agnew, D. C., & Cayan, D. R. (2014). Ongoing drought-induced uplift in the
 365 western United States. *Science*, *345*(6204), 1587-1590. doi:10.1002/wrcr.20173
- 366 Dixon, T. H. (1991). An introduction to the Global Positioning System and some geological
 367 applications. *Reviews of Geophysics*, *29*(2), 249-276.
- 368 EarthScope O&M Proposal. Retrieved from www.earthscope.org/about/printed_documents.html:
 369 Faunt, C. C., Sneed, M., Traum, J., & Brandt, J. T. (2016). Water availability and land
 370 subsidence in the Central Valley, California, USA. *Hydrogeology Journal*, *24*(3), 675-
 371 684. doi:10.1007/s10040-015-1339-x
- 372 Fu, Y., Argus, D. F., & Landerer, F. W. (2015). GPS as an independent measurement to estimate
 373 terrestrial water storage variations in Washington and Oregon. *Journal of Geophysical*
 374 *Research: Solid Earth*, *120*(1), 552-566. doi:10.1002/2014JB011415
- 375 GAGE Facility Proposal. Retrieved from www.unavco.org/highlights/2018/award.html:
 376 Hammond, W. C., Blewitt, G., & Kreemer, C. (2016). GPS Imaging of vertical land motion in
 377 California and Nevada: Implications for Sierra Nevada uplift. *Journal of Geophysical*
 378 *Research: Solid Earth*, *121*(10), 7681-7703. doi:10.1002/2016jb013458
- 379 Hammond, W. C., Burgette, R. J., Johnson, K. M., & Blewitt, G. (2018). Uplift of the Western
 380 Transverse Ranges and Ventura Area of Southern California: A Four-Technique Geodetic
 381 Study Combining GPS, InSAR, Leveling, and Tide Gauges. *Journal of Geophysical*
 382 *Research: Solid Earth*, *123*(1), 836-858. doi:10.1002/2017jb014499
- 383 Herring, T., King, R., & McClusky, S. (2015). Introduction to GAMIT/GLOBK, Release 10.6.
 384 Massachusetts Institute of Technology.
- 385 Herring, T. A., Melbourne, T. I., Murray, M. H., Floyd, M. A., Szeliga, W. M., King, R. W., et
 386 al. (2016). Plate Boundary Observatory and related networks: GPS data analysis methods
 387 and geodetic products. *Reviews of Geophysics*, *54*(4), 759-808.
 388 doi:10.1002/2016rg000529

- 389 Howell, S., Smith-Konter, B., Frazer, N., Tong, X., & Sandwell, D. (2016). The vertical
390 fingerprint of earthquake cycle loading in southern California. *Nature Geoscience*, 9,
391 611. doi:10.1038/ngeo2741
- 392 Johnson, C. W., Fu, Y., & Bürgmann, R. (2017). Seasonal water storage, stress modulation, and
393 California seismicity. *Science*, 356(6343), 1161-1164. doi:10.1126/science.aak9547
- 394 Kreemer, C., Hammond, W. C., & Blewitt, G. (2018). A Robust Estimation of the 3-D Intraplate
395 Deformation of the North American Plate From GPS. *Journal of Geophysical Research:*
396 *Solid Earth*, 123(5), 4388-4412. doi:10.1029/2017jb015257
- 397 Leveson, I. (2009). *Socio-Economic Benefits Study: Scoping the Value of CORS and GRAV-D*
398 *(report for National Geodetic Survey)*. Jackson, NJ: Leveson Consulting.
- 399 National Research Council. (2012). *Sea-Level Rise for the Coasts of California, Oregon, and*
400 *Washington: Past, Present, and Future*. Retrieved from Washington, DC:
401 doi:10.17226/13389
- 402 Neely, W. R., Borsa, A. A., & Silverii, F. (2020). GInSAR: A cGPS Correction for Enhanced
403 InSAR Time Series. *IEEE Transactions on Geoscience and Remote Sensing*, 58(1), 136-
404 146. doi:10.1109/TGRS.2019.2934118
- 405 Silver, P. G., Bock, Y., Agnew, D. C., Henyey, T., Linde, A. T., McEvelly, T. V., et al. (1998). A
406 plate boundary observatory. *IRIS Newsletter*, 16 (2), Fall/Winter.
- 407 Simpson, R. W., Thatcher, W., & Savage, J. C. (2012). Using cluster analysis to organize and
408 explore regional GPS velocities. *Geophysical Research Letters*, 39(18).
409 doi:10.1029/2012gl052755
- 410 Zeng, Y., Petersen, M. D., & Shen, Z.-K. (2018). Earthquake Potential in California-Nevada
411 Implied by Correlation of Strain Rate and Seismicity. *Geophysical Research Letters*,
412 45(4), 1778-1785. doi:10.1002/2017gl075967
- 413 Zumberge, J. F., Heflin, M. B., Jefferson, D. C., Watkins, M. M., & Webb, F. H. (1997). Precise
414 point positioning for the efficient and robust analysis of GPS data from large networks.
415 *Journal of Geophysical Research: Solid Earth*, 102(B3), 5005-5017.
416 doi:10.1029/96JB03860
417